Composites Science and Technology 243 (2023) 110250

Contents lists available at ScienceDirect

Composites Science and Technology

journal homepage: www.elsevier.com/locate/compscitech

Multifunctional nanocomposites reinforced by aligned graphene network via a low-cost lyophilization-free method

Shasha Wang [a,b,e,1], Yanjun Xu [a,d,1], Yu Ma [c,e], Xianxian Sun [b,c,e,**], Yongji Gong [b,c], Yibin Li [a,b,c,e,*]

[a] National Key Laboratory of Science and Technology on Advanced Composites in Special Environments, Harbin Institute of Technology, Harbin, 150080, PR China
[b] Tianmushan Laboratory, Hangzhou, 310023, PR China
[c] School of Materials Science and Engineering, Beihang University, Beijing, 100191, PR China
[d] Changchun Institute of Optics, Fine Mechanics and Physics, Chinese Academy of Sciences, Changchun, 130033, PR China
[e] Shandong Guoxi New Material Innovation Center Co., Ltd, Rizhao, 276800, PR China

ARTICLE INFO

Handling Editor: Prof. Y.-W. Mai

Keywords:
Lyophilization-free
Graphene aerogel
Long-range oriented structure
Thermal interface materials
Mechanical and electrical properties

ABSTRACT

Compared with a disordered network, the ordered framework is more beneficial to improving the multifunctional properties (including thermal, electrical, and mechanical properties) of epoxy-based composites. However, current methods for building aligned structures are both energy and time-consuming on account of the tedious and lengthy lyophilization process. Herein, a new strategy is proposed to obtain low-density graphene aerogels (GAs) with long-range oriented structures through a lyophilization-free processes. Due to the minimum thermal boundary resistance, the prepared aligned graphene/epoxy composite exhibits an ultrahigh thermal conductivity of ~11.6 W/(m·K) at a graphene content of 1.84 vol%, i.e., an enhancement efficiency of 3640% per 1 vol%. In addition, the compressive strength of the composite is increased by 2.6 times compared to epoxy (from 0.29 MPa to 0.76 MPa). Because the composite shows a modulus as low as 0.5–1.0 MPa, it has excellent deformability and compression performance. Moreover, the obtained 3-mm-thick composite achieves an electromagnetic interference shielding effectiveness (EMI SE) of 40 dB due to the interconnected graphene network structure, which meets the requirements of commercial EMI shielding applications. Hence, this strategy can be used to synthesize aligned graphene/epoxy composites with excellent multifunctional performances, which can be simultaneously used as elastic thermal interface materials (TIMs) and EMI shielding materials in the fields of advanced electronic packaging.

Credit author statement

Shasha Wang: Investigation, Conceptualization, Methodology, Data analysis, Writing-original draft, Software.

Yanjun Xu: Investigation, Data analysis, Supervision, Software, Writing-review & editing.

Yu Ma: Methodology, Data analysis, Writing-review & editing.

Xianxian Sun: Supervision, Methodology, Writing-review & editing.

Yongji Gong: Conceptualization, Supervision, Writing-review & editing.

Yibin Li: Conceptualization, Resources, Supervision, Validation, Writing-review & editing, Project administration.

1. Introduction

With the increasing integration of electronic devices, multifunctional thermal interface materials (TIMs) play an increasingly important role in their thermal management systems, which can enhance the heat transfer between interface gaps and shield electromagnetic interference (EMI) between various electronic components, meanwhile [1–5]. Polymer-based TIMs have excellent compressive properties and low modules, but the ultralow thermal and electrical conductivity severely

* Corresponding author. National Key Laboratory of Science and Technology on Advanced Composites in Special Environments, Harbin Institute of Technology, Harbin, 150080, PR China.
** Corresponding author. Tianmushan Laboratory, Hangzhou, 310023, PR China.
E-mail addresses: sunxx@buaa.edu.cn (X. Sun), liyibin@buaa.edu.cn (Y. Li).
[1] These authors contributed equally to the manuscript.

https://doi.org/10.1016/j.compscitech.2023.110250
Received 9 March 2023; Received in revised form 13 July 2023; Accepted 7 September 2023
Available online 9 September 2023

limits their practical applications [6–11]. Research shows that introducing high-thermal/electrical-conductivity fillers (copper, silver, aluminum oxide, carbon nanotubes, graphene, etc.) into the polymer matrix improves the multifunctional performance of polymer-based TIMs effectively [12–20]. Among them, graphene has attracted extensive attention due to its excellent mechanical property, thermal (5300 W/(m·K)) and electrical (10^8 S/m) conductivity [21–23].

As a typical 2D material, the in-plane and out-plane properties of graphene differ substantially. Hence, it needs to be aligned in the polymer matrix to give full play to its high thermal, electrical conductivity, and mechanical property, which has been widely proved by relevant studies [22–33]. For instance, Yu et al. [34] prepared a graphene/epoxy composite with highly aligned graphene via a directional-freezing process, which possesses a high electrical conductivity along the parallel direction even though the content of nanofillers is only 0.8 wt%. Kim et al. [35] produced a graphene pre-network using Ni foam to strengthen and toughen the epoxy matrix, and the obtained graphene/epoxy composite with cellular structure exhibited a simultaneous increase in flexural strength, flexural modulus, and fracture toughness. Yu et al. [30] prepared an epoxy composite reinforced with 0.75 vol% of highly-aligned graphene, which exhibited an excellent vertical thermal conductivity of 6.57 W/(m·K), and greatly improved storage modulus, compressive strength, and compressive strain at break. Despite this, the lyophilization process is usually required to fabricate these highly-aligned graphene networks, which is energy-intensive and time-consuming (require ultra-low temperature and vacuum condition, typically −50 °C, 10 Pa, 72 h) [28–30,36–38]. Hence, the development of efficient and energy-saving preparation methods for aligned-graphene-reinforced polymer matrix composites is of great significance for its large-scale application.

Here, we propose a lyophilization-free fabrication strategy for the synthesis of anisotropic graphene aerogels (GAs) with long-range aligned structures (Fig. 1a). A "fire-and-ice" method combining thermochemical reduction at 60–80 °C and direction-freezing was employed to synthesize an aligned reduced-GO (r-GO) hydrogel. The resulting r-GO hydrogel was air-dried under ambient conditions directly to obtain the arranged aerogel that was subsequently annealed at 2850 °C to remove the residual oxygen-containing groups and further repair the deficiencies. The as-prepared graphene/epoxy composite exhibited an ultrahigh thermal conductivity of ~11.6 W/(m·K) in the vertical direction at a graphene content of 1.84 vol%, that is, an enhancement efficiency of 3640% per 1 vol%. In addition, the compressive strength of the composite is increased by 2.6 times compared to epoxy (from 0.29 MPa to 0.76 MPa). The low modulus (0.5–1.0 MPa) indicates a good elastic performance of the composite, which can enhance the contact between two surfaces. Moreover, the electrical conductivity of the composites increased from 9.4×10^{-8} S/m (pure epoxy) to 830 S/m (composite with 1.84 vol% graphene), resulting in a substantial improvement in electromagnetic interference shielding effectiveness (EMI SE) of the composite (~40 dB) compared with the epoxy matrix (~3.5 dB). This study proposes a novel approach for fabricating aligned graphene/epoxy composites with superior multifunctional properties, which can serve as effective thermal interface materials (TIMs) and electromagnetic interference (EMI) shielding materials in advanced electronic packaging applications.

2. Experimental

2.1. Materials

Graphene oxide (GO) aqueous dispersion (16 mg/mL) was purchased from Hangzhou Gaoxi Technology Co., Ltd., and the average size of GO was ~10 μm characterized by transmission electron microscopy (TEM) (Fig. S1a). L-Ascorbic acid (L-AA) and epoxy (E51) were purchased from

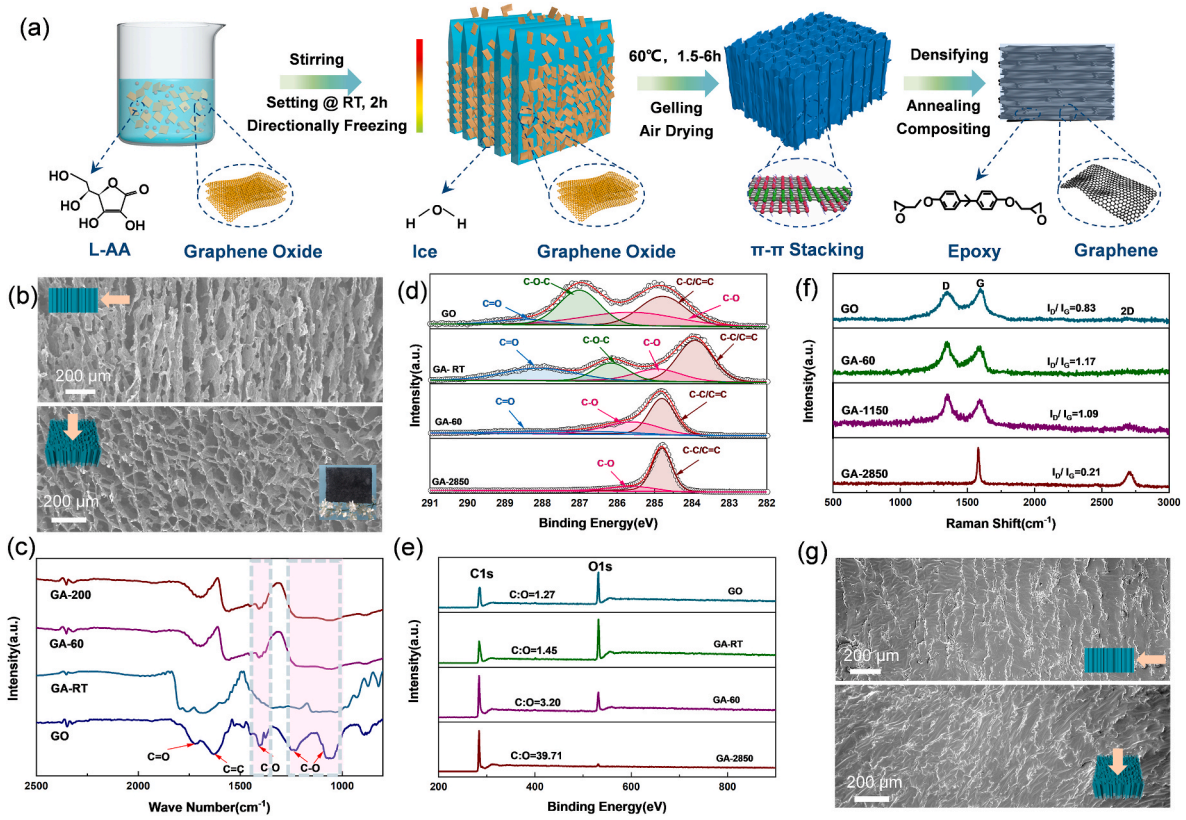

Fig. 1. (a) Schematic illustration of the fabrication procedure for GA. (b) The SEM images of aerogel vertical (Top) and horizontal direction (Down) (Inset the digital images for graphene aerogel) (c) FTIR spectra, (d)XPS, (e) C1s spectra, and (f) Raman spectra of GO with different treatment temperature. (g) The SEM images of composite vertical (Top) and horizontal direction (Down).

Tianjin Zhiyuan Technology Co., Ltd. and Hangzhou Wuhuigang Adhesive Co., Ltd., respectively.

2.2. Preparation of aligned GAs

As shown in Fig. 1a, the aligned GA was prepared using a lyophilization-free method, i.e., a combination of thermochemical reduction, directional freezing, and direct air drying. Herein, the environmentally friendly chemical reducing agent L-AA was used to realize the transition from GO solution to r-GO hydrogel. 80 g of GO aqueous dispersion and 4 g of L-AA were poured into a beaker and stirred for 5 min until L-AA was dissolved. The mixed solution was poured into a directional freezing module (80 × 80 × 15 mm^3) and stood for 1–2 h under ambient conditions (hereafter named GA-RT). The module was then immersed in an alcohol bath placed in the air above liquid nitrogen and frozen for 25–30 min. After thawing at 25–30 °C, the module was put into an oven with a cover and preliminarily reacted at 60 °C for ~2 h. After cooling to 25–30 °C, the preformed graphene hydrogel was subjected to a second directional freezing process. Then, the hydrogel was heated for further reaction at 60 °C for 4–6 h. The reaction at a mild temperature of 60 °C can avoid severe volume shrinkage caused by a rapid reduction reaction. The prepared graphene hydrogel was frozen at −20 °C for 4–6 h, then reacted at 60 °C for ~6h, 80 °C for ~4 h, washed with deionized water three to five times for the removal of residues, and fully dried at 60 °C in the air to obtain a graphene aerogel (hereafter named GA-60).

2.3. Preparation of aligned GA/epoxy composites

The obtained GA was annealed at 200 °C in the air for ~12 h (hereafter named GA-200) and 1150 °C under argon for ~2 h (hereafter named GA-1150) to remove the remaining L-AA, oxidized products, and further reduce the graphene oxide. Subsequently, the vertical GA was graphitized at 2850 °C for hours under argon to obtain high-quality GA (hereafter named GA-2850). The density of aerogel was adjusted through compression before graphitizing, which was increased from 14.9 to 41.6 mg/cm^3. The epoxy, curing agent and reactive diluent were thoroughly mixed with a mass ratio of 10:5:6, then the GA-2850 was immersed in the mixture in a vacuum oven for ~3 h. The obtained composite was cured at 60 °C for ~12 h (hereafter referred to as GA-2850/epoxy) and then cut into desired shapes for characterizations.

2.4. Materials characterization

Field-emission scanning electron microscopy (FESEM) (Carl Zeiss, Supra55) was performed on the GA and composite to investigate their morphology. A TENSOR 27 instrument (Bruker) was used for Fourier transform infrared (FTIR) measurement. Raman spectra and X-ray photoelectron spectroscopy (XPS) were performed on the samples to characterize their degree of reduction and repair using Lab RAM HR800 from Horiba (excited by a 532-nm laser) and ESAALAB 250Xi, respectively. The thermal conductivity of materials is calculated using $K = \alpha \times \rho \times C_p$, where α is the thermal diffusivity, ρ is the density, and C_p is the specific heat capacity. A Hotdisk TPS3500 was used to obtain the thermal parameters of GA-2850. And a Netzsch LFA457 light flash apparatus was used to measure the thermal diffusivities and specific heat capacities of the GA-2850/epoxy composites. The mechanical properties were tested using an Instron 5944. Infrared thermography was captured using an InfraTec VarioCAM HD head 880 thermographic system. The electrical conductivity was measured by Keithley 2461. The EMI SE was measured using an Agilent N5234A vector network analyzer in the frequency range of 10~15 GHz.

3. Results and discussion

Due to the nature of liquid crystals, the lateral size of the GO sheets (10 μm × 3 nm, Fig. S1a) used in this study is large enough to easily form aligned structure under the action of ice crystals [29,38,39]. During the reduction of GO sheets, the conjugate structure of GO sheets is restored and the π-π interaction between sheets is enhanced. The restored conjugation in graphene sheets promotes them to form extremely strong bindings among them, leading to their 3D self-assembly [40–42]. Once the hydrogel is fully formed, the shear force generated by ice crystal growth cannot overcome the strong interactions between disordered graphene sheets, making it challenging to achieve an orderly structure after complete gelation (Figs. S1b and S1c). Hence, it should be noted that directional freezing should be performed before full gelation to prevent the recovery of the π-π junction from hindering the ordered arrangement of GO sheets [39]. In addition, multiple and prolonged chemical reactions are necessary for the formation of robust π-π interactions between r-GO sheets, which can make the strength of the skeleton enough to prevent significant shrinkage caused by the large capillary pressure during the air-drying process. Furthermore, multi-freezing treatment before drying can strengthen the hydrogel skeleton, improve the attraction between sheets and avoid severe shrinkage. As depicted in Fig. 1b, the r-GO aerogels subjected to multi-freezing exhibit an oriented structure (the graphene sheets are arranged vertically), with the shrinkage being less than 12.5% (Figs. S1d and S1e). Conversely, the aerogels without multi-freezing treatment are deformed before drying caused by excessive shrinkage (the shrinkage rate is greater than 60%).

In order to reveal the evolution process of the GO chemical state, FTIR and XPS characterizations were performed on the aerogels with different reduction reaction states. As shown in Fig. 1c, the alkoxy C–O (1058 cm^{-1}), epoxy C–O (1228 cm^{-1}), and carboxy C–O (1402 cm^{-1}) peaks of GO dramatically declined and even disappeared with the reduction reaction with L-AA, indicating that L-AA can modify GO and realize the self-assembly of GO sheets based on π-π stacking due to the reduction of L-AA [43]. In addition, by characterizing the chemical states of GO, the arrangement of r-GO sheets can be controlled to achieve an aligned structure. The XPS results given in Fig. 1d and e shows the chemical transformation of GO under different treatments. After reacting with L-AA for 2 h at room temperature, the C/O atomic ratio increased moderately from 1.27 to 1.45, which shall be caused by the preliminary reduction of L-AA. When GO was further reduced by L-AA at 60 °C for hours, the C/O atomic ratio increased to 3.20 as most of the epoxy groups were removed, which was consistent with FTIR results. The C1 s spectrum in Fig. 1e reveals that the fractions of the carbonyl carbon C=O peak (~288.4 and 287.5 eV), epoxy carbon C–O–C peak (~286.6 eV), and hydroxyl carbon C–O peak (~285.6 eV) were decreased considerably compared with the C–C/C=C peak (~284.8 eV) due to the further reduction of r-GO [44,45]. These peaks assigned to oxygen-containing functional groups almost disappeared after graphitization, suggesting the complete reduction of GO, which is consistent with the significant increase of C/O atomic ratio to 39.71 in Fig. 1e. The above results indicate that L-AA can gradually reduce GO, and the ultra-high temperature annealing can further reduce and recover GO [30,46–48]. Since high-quality crystals are beneficial for heat and electrical transfer [36,49–51], Raman spectroscopy was performed to verify the evolution of crystalline quality in carbon-based materials. As shown in Fig. 1f, the samples have three peaks, namely, the G band (~1585 cm^{-1}), the D band (~1350 cm^{-1}), and the 2D band (~2700 cm^{-1}) [50]. The disappearance of some oxygen-containing functional groups after the reaction with L-AA created vacancies that increased the I_D/I_G ratio (a mark of defects and disordered structures in graphitic domains [30]) from 0.83 to 1.17. This indicates that r-GO needs further treatment to optimize the crystal structure for the improvement of heat transfer. The I_D/I_G ratio decreased sharply from 1.09 to 0.21 with the increase in the treatment temperature from 1150 °C to 2850 °C. This indicates that r-GO annealed at 2850 °C has better crystallinity and fewer defects than that at 1150 °C. Fig. 1g presents the microstructure of GA-2850/epoxy composite. Continuous and undeformed graphene

skeleton with aligned structure can be observed in the epoxy matrix, indicating the stable anisotropic structure of the aerogel due to the strong π-π stacking between graphene sheets. The reserved framework composed of aligned and interconnected graphene sheets can effectively enhance the comprehensive properties of the composite.

The arrangement of graphene sheets plays a crucial role in transforming the mechanical, electrical, and thermal properties of the graphene microstructure into the macrostructure of the graphene monolith [22]. In other words, the anisotropic structure results in significant variations in its performance along multiple several directions. Accordingly, compressive tests were performed in the vertical and horizontal directions of the aerogel to assess the anisotropic mechanical performance (Fig. 2a and Fig. S2a). Under the same strain, the compressive stress of GA-2850 in the vertical direction is relatively higher than that in the horizontal direction. Notably, after multiple cycles, the horizontal compressive stress of GA-2850 only decreased slightly for each strain (Fig. S2b), indicating that GA-2850 has excellent mechanical resilience. The digital images in Fig. 2a also show the recovery process of GA-2850 in the horizontal direction after multiple loading-unloading cycles. The height of GA-2850 almost returned to the original position after 100 cycles, and the residual strains are less than 12% under various strains (30%–90%, as shown in Fig. S2b, under 30% strain almost recovered completely). Thus, the GA has the potential as a flexible and compressible conductor (Fig. S2c). As shown in Fig. 2b, the vertical compressive stress of GA-2850 increased with the increase in density. Meanwhile, with the increase in density, the stress of GA-2850 in the horizontal direction is also enhanced, but there is a significant difference between it and the vertical direction. This is because when GA-2850 is compressed, the connected rigid graphene sheets can support the skeleton to improve mechanical strength along the vertical direction (Fig. 2c), but there is no such strengthening mechanism along the horizontal direction.

After compositing with aligned aerogel, the mechanical property of epoxy resin is enhanced by the supporting and bridging effects of aligned graphene sheets. The compressive strength of the composite in the vertical direction increased with the increase in graphene content (Fig. 2d), which can be attributed to the increase in the number of stiff and strong skeletons. When the graphene content increased from 0.66 vol% to 1.84 vol%, the compressive strength of the composite increased from 0.35 MPa to 0.76 MPa, which is 21%–162% higher than that of the pure epoxy resin. As is well-known, the ideal TIM shall have a low Young's modulus, which makes it easy to compress for pressure encapsulation and enhanced interface contact [52,53] And in typical electronics cooling applications, the pressure is of the order of 172 kPa or more [54], according to Fig. 2d left, the deformation of composite with GA-2850 can reach up to 20–40% under 200 kPa pressure. Moreover, the composite can be twisted like elastic epoxy shown in Fig. 2d inset, indicating that the GA-2850/epoxy composite tends to deform under pressure and can achieve full contact between interfaces. Although the modulus of the composite increased with increasing graphene content, due to the extremely low loading of graphene, even at a content of 1.84 vol%, the maximum modulus of the composite was still lower than 1.0 MPa, which is lower than conventional TIMs enhanced by metals (4–6 MPa) [55].

Due to the aligned and interconnected network, the structure will provide fast electron-transport channels and enhance the conductivity of the materials. As shown in Fig. 3a, the electrical conductivity of aerogel with density 14.4–41.4 mg/cm^3 is up to 230–950 S/m in the vertical direction, which exhibits an obvious distinction compared with that in the horizontal direction due to the anisotropy structure. The epoxy, when without fillers, is nearly an insulator with a low electrical conductivity of 9.4 × 10^{-8} S/m. However, after being composited with

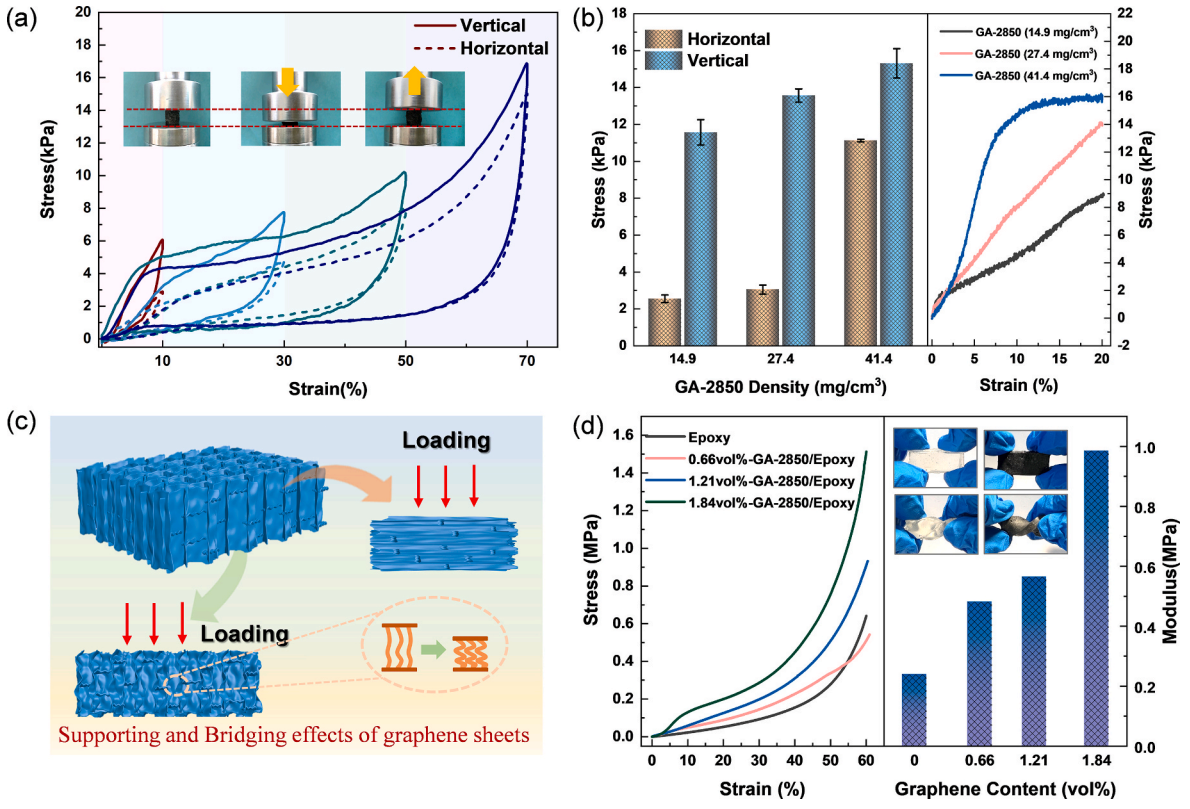

Fig. 2. (a) The curve of stress-strain for GA-2850 along different directions. (Inset the digital images for the process of unloading). (b)The compressive stress along the vertical and horizontal direction (Left) and the curve of stress-strain for GA-2850 with different densities along the vertical (Right). (c) Schematic illustration of deformation of GA-2850 in different directions for oriented structure. (d) The compressive stress-strain curve of GA-2850/epoxy and pure epoxy. (Left), the contrast diagram of elastic modulus (Right) (Inset the digital photo of torsional composites).

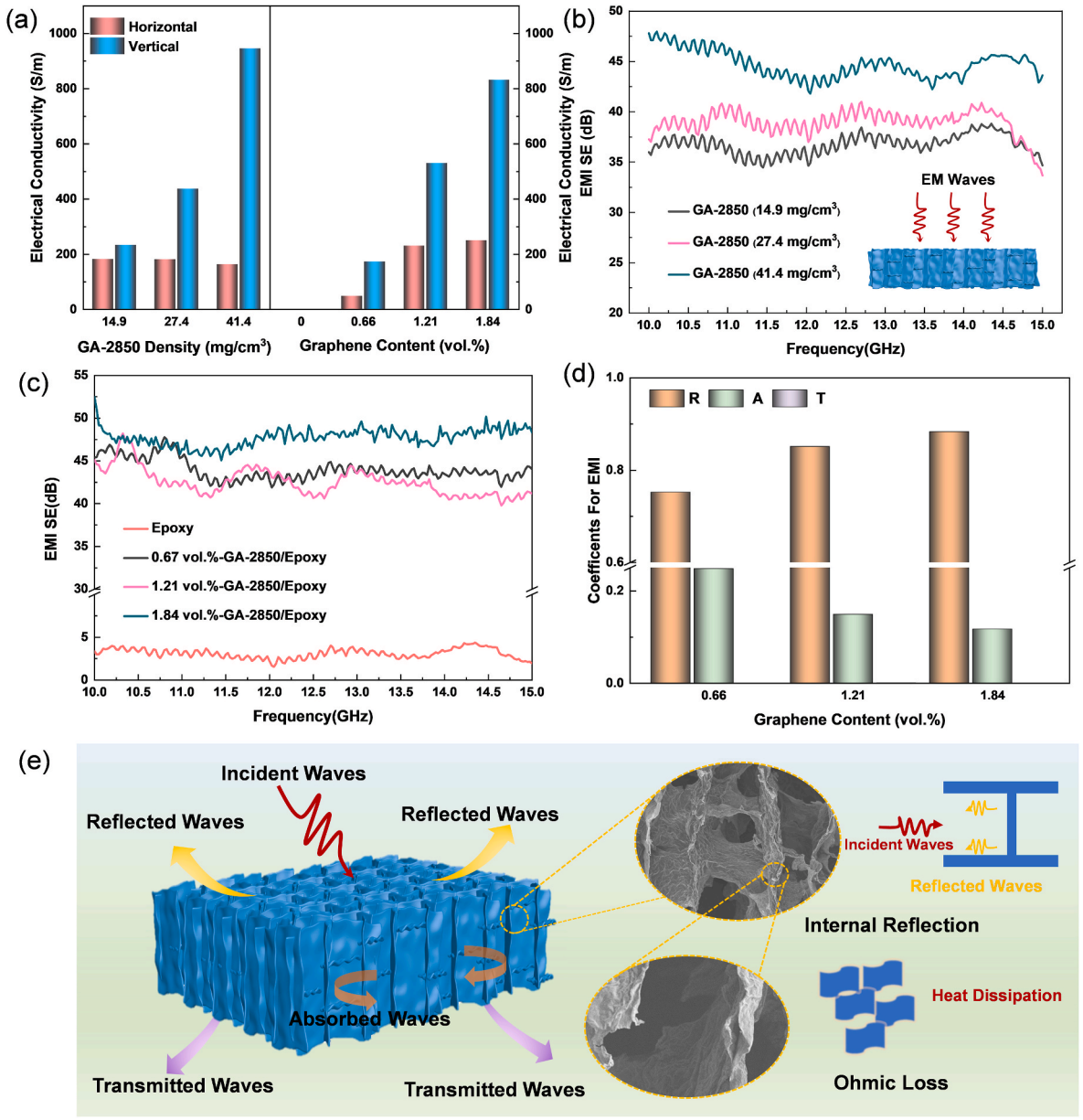

Fig. 3. (a) The electrical conductivity for GA-2850 with different densities (Left) and GA-2850/epoxy composites with different graphene loadings (Right) along vertical and horizontal directions. (b) The EMI SE for GA-2850 with different densities along vertical. (c) The EMI SE for GA-2850/epoxy with different graphene loadings along vertical. (d) The coefficients *R*, *T*, and *A* for GA-2850/epoxy with different graphene loadings along the vertical direction. (e) Schematic illustration of EMI shielding in the vertical direction for oriented structure.

aligned graphene aerogels, the conductivity of the composites increased to 170–830 S/m (Fig. 3a, with a graphene content of 0.66–1.84 vol%), indicating that the aligned and interconnected structure can improve the electron transport capacity of poor conductors. Due to the excellent electrical conductivity, the obtained GA-2850s exhibit an excellent EMI shielding ability (Fig. 3b). The EMI SE is calculated according to Schelkunoff's equation (Equations S1 to S7 in Supporting Information) [23,31,50]. For pure epoxy, the EMI SE is ~3.5 dB, which hardly meets the common requirement for EMI shielding application. However, the EMI SE for GA-2850s with a thickness of 3 mm is higher than 20 dB (minimum 30 dB in the vertical direction as exhibited in Fig. 3c). After being composited with the GA-2850, which has excellent EMI shielding properties, the EMI SE of the GA-2850/epoxy composite is improved to ~40 dB. It is about 10 times higher than that of epoxy, indicating that the EMI shielding property of composite is enhanced by the synergistic effect of graphene and epoxy. Furthermore, increasing the loading of graphene in composites can further enhance the EMI SE.

To analyze the mechanism of shielding, the EM parameters *R* (reflection coefficient), *T* (transmission coefficient), and *A* (absorption coefficient) for the composites are calculated (Fig. 3d). In Fig. S3, the order of the *T* value is 10^{-5} for GA-2850/epoxy composites with different graphene loadings, indicating that the shielding efficiency of the composite can reach up to 99.99%. As given in Fig. 3d, the *R* is raised with the increase of graphene content, which should be ascribed to the intensification of impedance mismatching between GA-2850/epoxy and air causing more EM waves to be reflected [31]. Moreover, the electric conductive frameworks constructed by interconnected GA-2850 provide an efficient pathway for charge transfer, resulting in strong EM reflection through the excitation of high-frequency oscillating current [56]. Thus, 75.2%, 85.1%, and 88.3% of the incident EM waves are reflected at the surface for 0.66 vol%, 1.21 vol%, and 1.84 vol%-GA-2850/epoxy, respectively. As depicted in Fig. 3e, the residual EM wave penetrates the

porous skeleton composed of interconnected aerogel and undergoes attenuation due to multiple internal reflections and scattering between sheets. Meanwhile, the interconnected graphene sheets also provide numerous dipoles that dissipate EM waves as thermal energy, demonstrating an excellent EMI shielding capability [56,57].

As discussed above, the vertical pathway not only facilitates effective electron transport but also enhances thermal properties by providing fast phonon-transport channels. Additionally, for an ideal TIM, high thermal conductivity is also essential to decrease the interfacial thermal resistance [58]. Compared with the horizontal and random systems, the vertical direction demonstrates superior thermal performance, as illustrated in Fig. S4. After 5 min of heating at the bottom, the temperature of the composite with the vertical graphene is about 16.2 °C and 5.3 °C higher than those with horizontal and random structures, respectively, highlighting the critical role of fillers' arrangement in efficient heat transfer.

To further investigate the actual performance of aligned GA-2850, the thermal conductivity K was measured in different directions. As illustrated in Fig. 4a, the K shows anisotropic behavior after graphitization, moreover, the K value increases with the rise of graphene content due to the increase in the number of heat conduction channels per cross-sectional area. This is consistent with the simulation results in Fig. S4b. When the density of GA-2850 reaches 41.4 mg/cm^3, the K value in the vertical direction increases to ~9.6 W/(m·K), which differs significantly from that in the horizontal direction. Due to the excellent vertical thermal property of GA-2850, its K value increased from 0.17 W/(m·K)

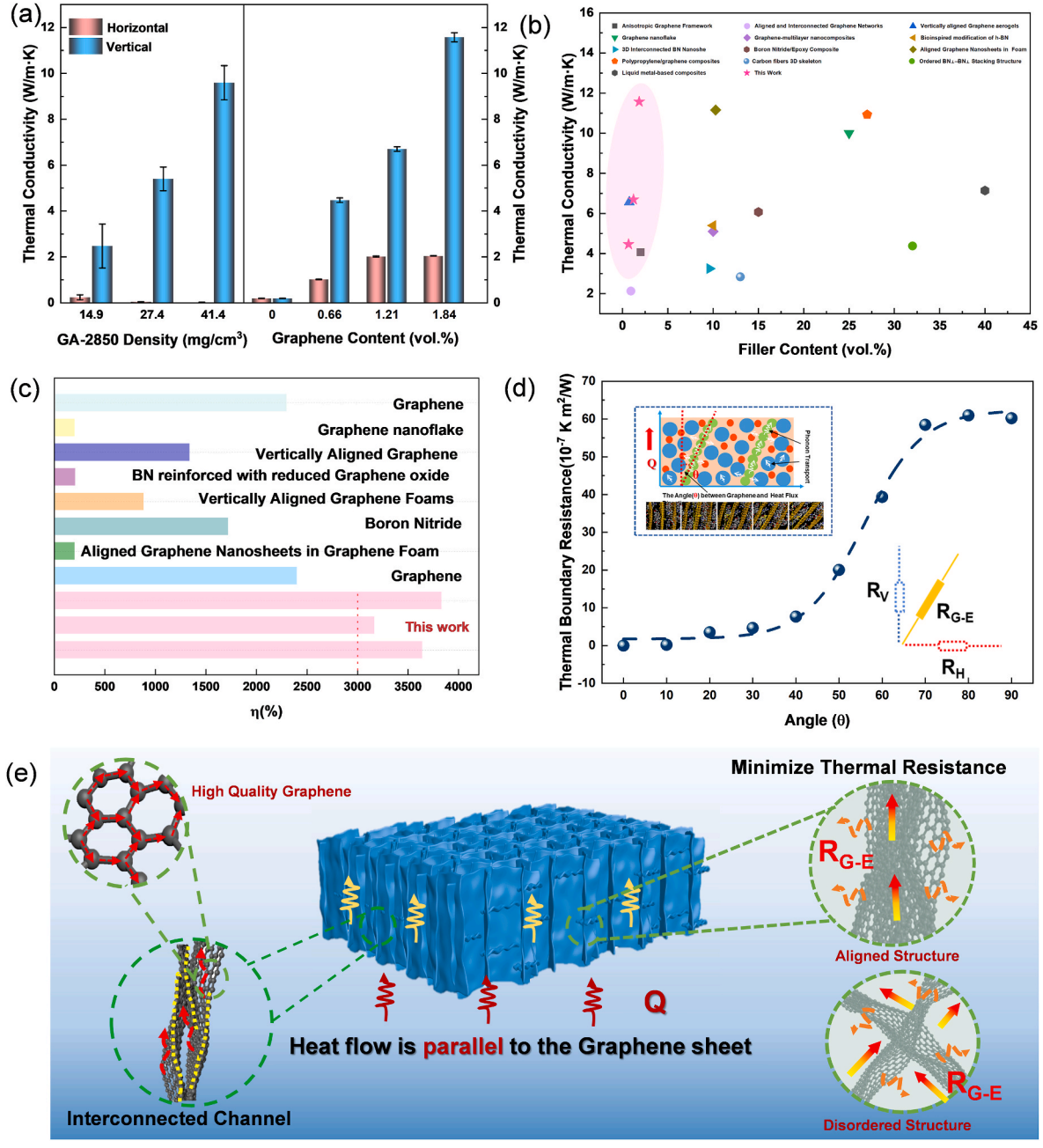

Fig. 4. (a) The thermal conductivity K for GA-2850 with different densities (Left) and GA-2850/epoxy composites with different graphene loadings (Right) along vertical and horizontal directions. (b) The thermal conductivity and (c) enhancement efficiency comparisons with the reported article. (d) The thermal boundary resistance of composites simulated by FEM and EMT, (Inset left the illustration diagram for angles of the composites reinforced by graphene. Inset right the decomposition of boundary). (e) Schematic illustration of heat transfer in the vertical direction for oriented structure and three-dimension random structure.

of pure resin to 4.6–11.6 W/(m·K) of GA-2850/epoxy composites containing 0.66–1.84 vol% graphene. Compared with previous results for composites with high K fillers, the obtained GA-2850/epoxy composites demonstrate significantly superior thermal performance despite ultra-low graphene content (Fig. 4b).

To eliminate the influence of filler loading, Equation (1) was used for calculating the thermal conductivity enhancement efficiency (η) [36].

$$\eta = \frac{K - K_M}{100 f K_M} \times 100\% \tag{1}$$

In this equation, K and K_M are the thermal conductivities of the composites and polymer matrix, respectively, and f is the volume fraction of fillers. As shown in Fig. 4c, the GA-2850/epoxy composites have higher enhancement efficiency compared with the previously reported ones [27,29,30,36,59–68]. The GA-2850/epoxy composite with 1.84 vol% graphene loading exhibits an enhancement efficiency of 3640% per 1 vol %, indicating the aligned graphene obtained in this study can significantly enhance heat transfer capacity.

Both the effective medium theory (EMT) model and the Foygel model are utilized to analyze various factors that affect thermal properties, such as size, morphology, content, distribution of fillers, and thermal resistance between fillers as well as between fillers and matrix. Compared with the Foygel model, which describes the quantitative relationship between the overlapping area of the adjacent graphene sheets and the thermal conductivity of the graphene skeleton [27], the EMT model is better suitable for analyzing the influence of fillers' arrangement on the effective thermal conductivity K^* of the composites [1,30,69]. The graphene channel could be assumed as flat plate inclusions when only the distribution of graphene sheets is considered, and the thermal conductivity can be calculated by using:

$$K_{11}^* = K_{22}^* = K_{\mathrm{M}} \frac{2 + f\left[\frac{K_G - K_M}{K_M}(1 + <\cos^2\theta>)\right]}{2 - f\left[\left(1 - \frac{R_{G-E}K_M}{h} - \frac{K_M}{K_G}\right)(1 - <\cos^2\theta>)\right]} \tag{2}$$

$$K_{33}^* = K_{\mathrm{M}} \frac{1 + f\left(\frac{K_G - K_M}{K_M}\right)(1 - <\cos^2\theta>)}{1 - f\left(1 - \frac{R_{G-E}K_M}{h} - \frac{K_M}{K_G}\right) <\cos^2\theta>} \tag{3}$$

Where K and K are the thermal conductivities along the vertical and horizontal directions, respectively. K_M and K_G are the thermal conductivities of the polymer matrix and graphene, respectively, $R_{G\text{-}M}$ is the thermal boundary resistance between the polymer and graphene, h is the thickness of the graphene sheet, f is the volume fraction of fillers, and θ represents the angle between the orientation of graphene sheets and the direction of heat flux (from hot to cold) as illustrated in the left inset in Fig. 4d. Equation (2) indicates that when $<cos^2\theta> \neq 1$ (the graphene inclusions are not aligned with the heat flux direction), $R_{G\text{-}M}$ must be taken into account to calculate the vertical K. However, when the graphene inclusions are parallel to the heat flux, $<cos^2\theta> = 1$, the effective thermal conductivity K^* can be expressed as follows:

$$K_{11}^* = K_{22}^* = fK_G + (1 - f)K_M \tag{4}$$

$$K_{33}^* = \frac{K_{\mathrm{M}}}{1 - f\left(1 - \frac{R_{G-E}K_M}{h} - \frac{K_M}{K_G}\right)} \tag{5}$$

According to Equation (4), when heat flow is parallel to the aligned graphene sheets, the effective thermal conductivity K^* is solely determined by the thermal conductivity of materials and their content, regardless of the thermal boundary resistance between graphene and polymer. And the theoretical thermal conductivities of GA-2850/epoxy, as calculated using the EMT model, are consistent with the experimental results in the vertical direction when K_G is 600 W/(m·K) and K_M is 0.17 W/(m·K), as illustrated in Fig. S5a. It should be noted that K_G is determined from the experimental thermal conductivities of composites rather than the theoretical value of graphene due to the contact thermal resistance between graphene sheets caused by overlap, which can be evaluated using the Foygel model as shown in Fig. S5b. To further investigate the impact of thermal boundary resistance between graphene and polymer on the thermal conductivity of the composites, the K value of polymer composites reinforced by arranged graphene was studied by the finite element method (FEM) (Fig. S6a). To simplify the subsequent calculations and analysis, the ideal oriented structures were modeled by assuming that the graphene is a flat plate with varying angles from the heat flux (defined as θ). As θ increases from 0° to 90°, the K decreases from 15.55 to 0.17 W/(m·K), indicating the significant impact of the arrangement of graphene sheets on thermal conductivity. Considering the angle between the arrangement of graphene sheets and heat flow, the interface thermal resistance between graphene and polymer, which is calculated using Equation (2), increases from 2×10^{-8} to 6×10^{-6} K m^2/W with an increase of θ as shown in Fig. 4d, indicating a negative correlation between high thermal boundary resistance and low thermal conductivity. In general, the total boundary between graphene sheets and polymer can be categorized into horizontal and vertical interfaces when the heat flow is not parallel to the graphene sheet (the right inset in Fig. 4d). The horizontal boundary perpendicular to the heat flux will create a barrier for phonon propagation in the vertical direction due to the mismatch of phonon mode, resulting in phonon scattering and high thermal resistance that regulate the "direction" of heat transfer (always along the direction of the high-thermal-conductivity graphene sheets, as shown in Fig. S6b). Therefore, an aligned channel parallel to heat flow is desirable to minimize thermal boundary resistance and improve heat transfer.

In summary, as demonstrated in Fig. 4e, the excellent thermal properties of composites enhanced by aligned graphene arise from these points: (I) The transfer of phonon of the aligned framework is most efficient compared to the other structures due to the minimum thermal boundary resistance. (II) As presented in Fig. S7, the interconnected pathway formed by graphene sheets through strong π-π interactions provides continuous channels for phonon vibration transportation [54,70,71]. (III) High-quality graphene can reduce phonon scattering during transport, thereby enhancing thermal conductivity [29,30,33]. However, for random interconnected networks, phonon scattering at the numerous interfaces due to the mismatch of phonon mode leads to significant thermal resistance and greatly reduces the thermal conductivity. Therefore, the aligned GA-2850/epoxy composite can exhibit superior thermal performance.

The special non-isotropic structure endows the graphene aerogel and composite discrepant characteristics of performance in different directions, making the anisotropic aerogel and aerogel/epoxy composites suitable for various situations. As shown in Fig. 5a, GA-2850 was placed on a copper block submerged in liquid nitrogen. In comparison to the horizontal orientation, the water droplet situated on the surface perpendicular to the arrangement of graphene sheets underwent complete freezing within 60 s (at least 90 s for the horizontal orientation). As shown in Fig. 5b, GA-2850 exhibits distinct temperature distributions along the vertical and horizontal directions at the same height. The temperature difference between these two directions is 3.6°C (Fig. 5c), which further confirms the anisotropic heat transfer caused by the oriented arrangement of graphene sheets. The anisotropic aerogel is expected to be used in the field of rapid heat transfer (vertical structure) or anti-heat insulation (horizontal structure).

Due to the exceptional multifunction of the aligned-graphene-aerogel-reinforced nanocomposites, the GA-2850/epoxy composites can serve as novel TIMs to reduce interfacial thermal resistance and EMI pollution, meanwhile. Compared with commercial silicone thermal pad BL-400 with a K of 3.5–5 W/(m·K), the GA-2850/epoxy composites exhibit better heat transfer capacity. As shown in Fig. 5d–e, the temperature of the copper block placed on the GA-2850/epoxy composite rises faster than that on the BL-400 (with a bottom temperature of 45 °C). After 600 s of operation, the temperature of the block on the

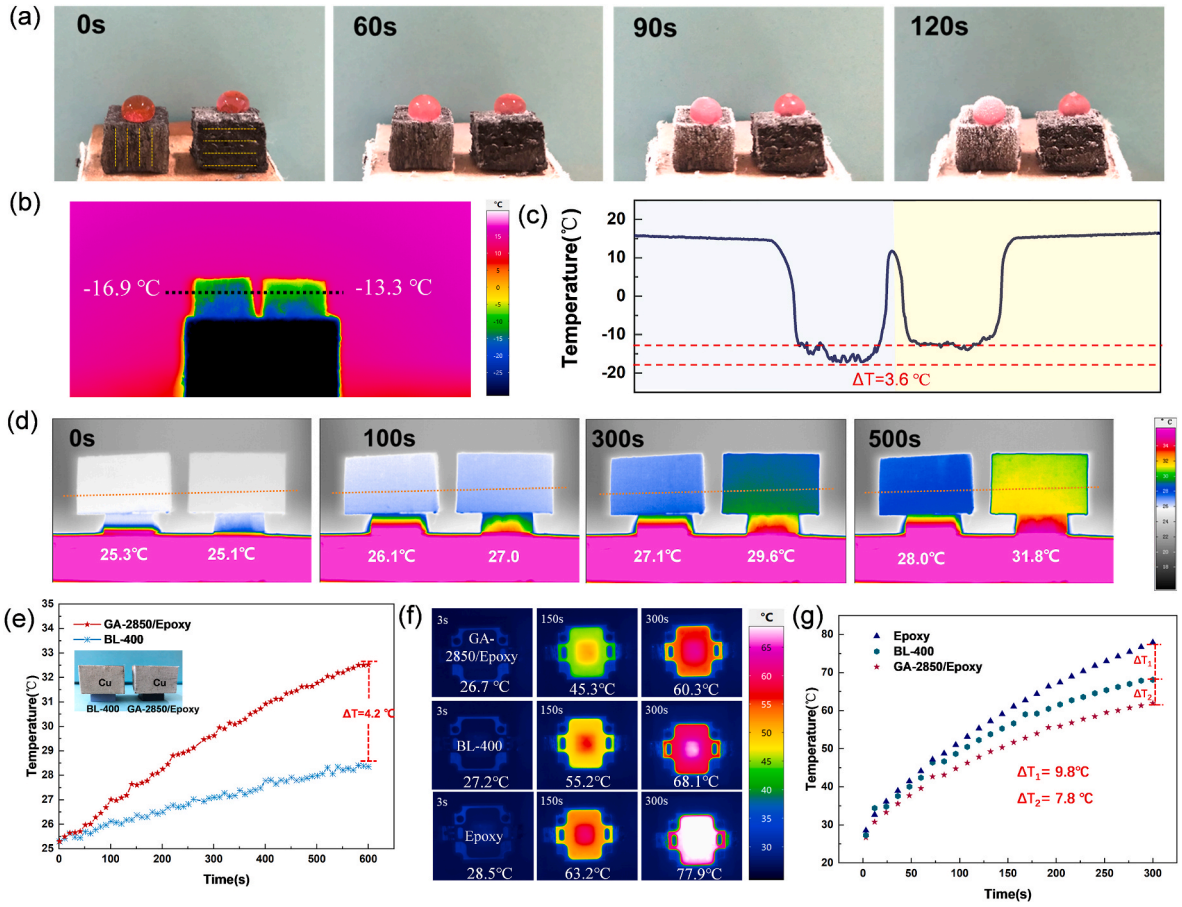

Fig. 5. (a) The digital photos of the thermal transfer ability of GA-2850 along vertical (Left) and horizontal (Right) directions at different times in a cold environment. (b) The thermographic image and (c) the temperature distribution of GA-2850 placed on a block of copper immersed in liquid nitrogen for 60 s. (d) The thermographic images and (e) time-temperature curves of GA-2850/epoxy (Left) and commercial thermal pad BL-400 (Right) on a 45 °C hot plate (Inset the digital image for the comparison of GA-2850/epoxy and BL-400) (f) The infrared thermal images showing the heat dissipation of a high-power LED and (g) the temperature-time curves of different TIMs.

composite was about 4 °C higher than that placed on BL-400, indicating that the GA-2850/epoxy has excellent heat transfer to enhance interfacial heat transfer. To visually demonstrate the practical performance in thermal management, 1.84 vol%-GA-2850/epoxy composite, BL-400, and pure epoxy were used as TIMs between a 10 W LED chip and a copper heat sink. When using composite material as the TIM, the surface temperature of LED lamp was 60.5°C after running for 300 s, which was lower than BL-400 and pure epoxy resin 7.8°C and 17.6°C, respectively (Fig. 5f–g). This suggests that the aligned structure endows the GA-2850/epoxy composite with reliable heat transfer ability, highlighting the advantages for thermal management applications as a multifunctional TIM.

4. Conclusions

In summary, the GA with a highly anisotropic structure has been fabricated using a lyophilization-free method. The vertically aligned 2D graphene sheets build highly efficient thermal conductance pathways along the vertical direction of GAs, maximizing the vertical thermal conductivity of polymer/GA composites. The GA-2850/epoxy composite with 1.84 vol% graphene exhibits an ultrahigh thermal conductivity of ~11.6 W/(m·K) along the vertical direction (an enhancement efficiency of approximately 3640% per 1 vol%). In addition to the thermal property, the GA-2850/epoxy composites with the ultralow graphene loading also have outstanding mechanical properties (compression strength 0.33–0.76 MPa) compared to neat epoxy (0.29 MPa). The modulus of the composite is as low as 1.0 MPa, indicating that the composite has excellent compressive performance. Meanwhile, the electrical conductivity of composites is enhanced from 9.4×10^{-8} S/m (pure epoxy) to 830 S/m (with 1.84 vol% graphene content), the EMI SE for composites is all above ~40 dB (~3.5 dB for epoxy). These excellent thermal, mechanical, and electrical properties indicate that the aligned graphene-epoxy composites prepared by this strategy can be used as multifunctional TIMs in advanced electronic packaging to solve complex problems between interfaces.

Declaration of competing interest

The authors declare that they have no known competing financial interests or personal relationships that could have appeared to influence the work reported in this paper.

Data availability

No data was used for the research described in the article.

Acknowledgments

This manuscript was financially sponsored by the National Natural Science Foundation of China (Grant No. 51772063) and the National Natural Science Foundation Youth Fund Program (Grant No. 52201166).

Appendix A. Supplementary data

Supplementary data to this article can be found online at https://doi.org/10.1016/j.compscitech.2023.110250.

References

[1] Q. Li, Y.F. Guo, W.W. Li, S.Q. Qiu, C. Zhu, X.F. Wei, M.L. Chen, C.J. Liu, S.T. Liao, Y.P. Gong, A.K. Mishra, L.W. Liu, Ultrahigh thermal conductivity of assembled aligned multilayer graphene/epoxy composite, Chem. Mater. 26 (15) (2014) 4459–4465.

[2] Y.S. Zhao, D. Liu, J. Chen, L.Y. Zhu, A. Belianinov, O.S. Ovchinnikova, R.R. Unocic, M.J. Burch, S.K. Kim, H.F. Hao, D.S. Pickard, B.W. Li, J.T.L. Thong, Engineering the thermal conductivity along an individual silicon nanowire by selective helium ion irradiation, Nat. Commun. 8 (2017), 15919.

[3] D.M. Hu, W.B. Gong, J.T. Di, D. Li, R. Li, W.B. Lu, B.H. Gu, B.Z. Sun, Q.W. Li, Strong graphene-interlayered carbon nanotube films with high thermal conductivity, Carbon 118 (2017) 659–665.

[4] K. Chu, X.H. Wang, Y.B. Li, D.J. Huang, Z.R. Geng, X.L. Zhao, H. Liu, H. Zhang, Thermal properties of graphene/metal composites with aligned graphene, Mater. Des. 140 (2018) 85–94.

[5] H.F. Song, J.M. Liu, B.L. Liu, J.Q. Wu, H.M. Cheng, F.Y. Kang, Two-Dimensional materials for thermal management applications, Joule 2 (2018) 442–463.

[6] K.M. Razeeb, E. Dalton, G.L.W. Cross, A.J. Robinson, Present and future thermal interface materials for electronic devices, Int. Mater. Rev. 63 (1) (2017) 1–21.

[7] W.Y. Zhang, Q.Q. Kong, Z.C. Tao, J.C. Wei, L.J. Xie, X.Y. Cui, C.M. Chen, 3D thermally cross-linked graphene aerogel–enhanced silicone rubber elastomer as thermal interface, Material. Advanced Materials Interfaces. 6 (12) (2019), 1970080.

[8] H.T. Yu, Y.Y. Feng, C. Chen, Z.X. Zhang, Y. Cai, M.M. Qin, W. Feng, Thermally conductive, self-healing, and elastic Polyimide@Vertically aligned carbon nanotubes composite as smart thermal interface material, Carbon 179 (2021) 348–357.

[9] X.F. Xu, J. Chen, J. Zhou, B.W. Li, Thermal conductivity of polymers and their nanocomposites, Adv. Mater. 30 (17) (2018), 1705544.

[10] F. Zhang, Y.Y. Feng, W. Feng, Three-dimensional interconnected networks for thermally conductive polymer composites: design, preparation, properties, and mechanisms, Mater. Sci. Eng. R Rep. 142 (2020), 100580.

[11] X.F. Xu, J. Zhou, J. Chen, Thermal transport in conductive polymer–based materials, Adv. Funct. Mater. 30 (8) (2020), 1904704.

[12] M. Li, M.J. Wang, X. Hou, Z.L. Zhan, H. Wang, H. Fu, C.T. Lin, L. Fu, N. Jiang, J. H. Yu, Highly thermal conductive and electrical insulating polymer composites with boron nitride, Compos. B Eng. 184 (2020), 107746.

[13] L. Cheng, J.C. Feng, Flexible and fire-resistant all-inorganic composite film with high in-plane thermal conductivity, Chem. Eng. J. 398 (2020), 125633.

[14] X.X. Guo, S.J. Cheng, W.W. Cai, Y.F. Zhang, X.A. Zhang, A review of carbon-based thermal interface materials: mechanism, thermal measurements and thermal properties, Mater. Des. 209 (2021), 109936.

[15] B. Shin, S. Mondal, M. Lee, S. Kim, Y. Huh, C. Nah, Flexible thermoplastic polyurethane-carbon nanotube composites for electromagnetic interference shielding and thermal management, Chem. Eng. J. 418 (2021), 129282.

[16] C.M. Ajmal, A.P. Benny, W. Jeon, S. Kim, S.W. Kim, S. Baik, In-situ reduced non-oxidized copper nanoparticles in nanocomposites with extraordinary high electrical and thermal conductivity, Mater. Today 48 (2021) 59–71.

[17] J. Khan, S.A. Momin, M. Mariatti, A review on advanced carbon-based thermal interface materials for electronic devices, Carbon 168 (2020) 65–112.

[18] F. Zhang, Y.Y. Feng, M.M. Qin, L. Gao, Z.Y. Li, F.L. Zhao, Z.X. Zhang, F. Lv, W. Feng, Stress controllability in thermal and electrical conductivity of 3D elastic graphene-crosslinked carbon nanotube sponge/polyimide nanocomposite, Adv. Funct. Mater. 29 (25) (2019), 1901383.

[19] H.T. Yu, C. Chen, J.X. Sun, H. Zhang, Y.Y. Feng, M.M. Qin, W. Feng, Highly thermally conductive polymer/graphene composites with rapid room-temperature self-healing capacity, Nano-Micro Lett. 14 (2022) 135.

[20] H.T. Yu, Y.Y. Feng, L. Gao, C. Chen, Z.X. Zhang, W. Feng, Self-Healing high strength and thermal conductivity of 3D graphene/PDMS composites by the optimization of multiple molecular interactions, Macromolecules 53 (2020) 7161–7170.

[21] J.Y. Gao, Q.W. Yan, L. Lv, X. Tan, J.F. Ying, K. Yang, J.H. Yu, S.Y. Du, Q.P. Wei, R. Xiang, Y.G. Yao, X.L. Zeng, R. Sun, C.P. Wong, N. Jiang, C.T. Lin, W. Dai, Lightweight thermal interface materials based on hierarchically structured graphene paper with superior through-plane thermal conductivity, Chem. Eng. J. 419 (2021), 129609.

[22] S.C. Xu, J. Zhang, Vertically aligned graphene for thermal interface materials, Small Structures 1 (3) (2020), 2000034.

[23] H.M. Fang, H.C. Guo, Y.R. Hu, Y.J. Ren, P.C. Hsu, S.L. Bai, In-situ grown hollow Fe_3O_4 onto graphene foam nanocomposites with high EMI shielding effectiveness and thermal conductivity, Compos. Sci. Technol. 188 (2020), 107975.

[24] H.F. Zhan, Y.H. Nie, Y.N. Chen, J.M. Bell, Y.T. Gu, Thermal transport in 3D nanostructures, Adv. Funct. Mater. 30 (2020), 1903841.

[25] A. Akbari, B.V. Cunning, S.R. Joshi, C.H. Wang, D.C. Camacho-Mojica, S. Chatterjee, V. Modepalli, C. Cahoon, C.W. Bielawski, P. Bakharev, G.H. Kim, R. S. Ruoff, Highly ordered and dense thermally conductive graphitic films from a graphene oxide/reduced graphene oxide mixture - ScienceDirect, Matter 2 (5) (2020) 1198–1206.

[26] X. Tan, J.F. Ying, J.Y. Gao, Q.W. Yan, L. Lv, K. Nishimura, Q.P. Wei, H. Li, S.Y. Du, B. Wu, R. Xiang, J.H. Yu, N. Jiang, C.T. Lin, W. Dai, Rational design of high-performance thermal interface materials based on gold-nanocap-modified vertically aligned graphene architecture, Compos. Commun. 24 (2021), 100621.

[27] W. Dai, L. Lv, T.F. Ma, X.Z. Wang, J.F. Ying, Q.W. Yan, X. Tan, J.Y. Gao, C. Xue, J. H. Yu, Y.G. Yao, Q.P. Wei, R. Sun, Y. Wang, T.H. Liu, T. Chen, R. Xiang, N. Jiang, Q. J. Xue, C.P. Wong, S. Maruyama, C.T. Lin, Multiscale structural modulation of anisotropic graphene framework for polymer composites achieving highly efficient thermal energy management, Adv. Sci. 8 (7) (2021), 2003734.

[28] S.C. Xu, S.S. Wang, Z. Chen, Y.Y. Sun, Z.F. Gao, H. Zhang, J. Zhang, Electric-field-assisted growth of vertical graphene arrays and the application in thermal interface materials, Adv. Funct. Mater. 30 (34) (2020), 2003302.

[29] X.X. Sun, C.J. Huang, L.D. Wang, L.L. Liang, Y.J. Cheng, W.D. Fei, Y.B. Li, Recent progress in graphene/polymer nanocomposites, Adv. Mater. 33 (2020), 2001105.

[30] X.H. Li, P.F. Liu, X.F. Li, F. An, P. Min, K.N. Liao, Z.Z. Yu, Vertically aligned, ultralight and highly compressive all-graphitized graphene aerogels for highly thermally conductive polymer composites, Carbon 140 (2018) 624–633.

[31] R. Shen, M. Weng, L. Zhang, J. Huang, X. Sheng, Biomass-based carbon aerogel/Fe_3O_4@PEG phase change composites with satisfactory electromagnetic interference shielding and multi-source driven thermal management in thermal energy storage, Compos. Appl. Sci. Manuf. 163 (2022), 107248.

[32] G. Lian, C.C. Tuan, L.Y. Li, S.L. Jiao, Q.L. Wang, K.S. Moon, D.L. Cui, C.P. Wong, Aligned and interconnected graphene networks for high thermal conductivity of epoxy composites with ultralow loading, Chem. Mater. 28 (2016) 6096–6104.

[33] QiY. Peng, Y.Y. Qin, X. Zhao, X.X. Sun, Q. Chen, F. Xu, Z.S. Lin, Y. Yuan, Y. Li, J. J. Li, W.L. Yin, C. Gao, F. Zhang, X.D. He, Y.B. Li, Superlight, mechanically flexible, thermally superinsulating, and antifrosting anisotropic nanocomposite foam based on hierarchical graphene oxide assembly, ACS Appl. Mater. Interfaces 9 (50) (2017) 44010–44017.

[34] X.H. Li, X.F. Li, K.N. Liao, P. Min, T. Liu, A. Dasari, Z.Z. Yu, Thermally annealed anisotropic graphene aerogels and their electrically conductive epoxy composites with excellent electromagnetic interference shielding efficiencies, ACS Appl. Mater. Interfaces 8 (2016) 33230–33239.

[35] J.J. Jia, X.Y. Sun, X.Y. Lin, X. Shen, Y.W. Mai, J.K. Kim, Exceptional electrical conductivity and fracture resistance of 3D interconnected graphene foam/epoxy composites, ACS Nano 8 (6) (2014) 5774–5783.

[36] F. An, X.F. Li, P. Min, P.F. Liu, Z.G. Jiang, Z.Z. Yu, Vertically aligned high-quality graphene foams for anisotropically conductive polymer composites with ultrahigh through-plane thermal conductivities, ACS Appl Mater Interfaces. ACS Appl Mater Interfaces. 10 (20) (2018) 17383–17392.

[37] H.Y. Ma, H.Y. Geng, B.W. Yao, M.M. Wu, C. Li, M. Zhang, F.Y. Chi, L.T. Qu, Highly ordered graphene solid: an efficient platform for capacitive sodium-ion storage with ultrahigh volumetric capacity and superior rate capability, ACS Nano 13 (2019) 9161–9170.

[38] P.F. Liu, X.F. Li, P. Min, X.Y. Chang, C. Shu, Y. Ding, Z.Z. Yu, 3D lamellar-structured graphene aerogels for thermal interface composites with high through-plane thermal conductivity and fracture toughness, Nano-Micro Lett. 13 (22) (2021) 13–27.

[39] H.S. Yang, Z.L. Li, B. Lu, J. Gao, X.T. Jin, G.Q. Sun, G.F. Zhang, P.P. Zhang, L.T. Qu, Reconstruction of inherent graphene oxide liquid crystals for large-scale fabrication of structure-intact graphene aerogel bulk toward practical applications, ACS Nano 12 (11) (2018) 11407–11416.

[40] J.L. Zhang, H.J. Yang, G.X. Shen, P. Cheng, J.Y. Zhang, S.W. Guo, Reduction of graphene oxide via L-ascorbic acid, Chem. Commun. 46 (2010) 1112–1114.

[41] H.S. Yang, J.M. Zhang, M. Jiang, T.P. Zhang, Y.X. Duan, Ambient pressure dried graphene aerogels with superelasticity and multifunctionality, J. Mater. Chem. A 3 (2015), 19268.

[42] K.X. Sheng, Y.X. Xu, C. Li, G.Q. Shi, High-performance self-assembled graphene hydrogels prepared by chemical reduction of graphene oxide, N. Carbon Mater. 26 (1) (2011) 9–15.

[43] Y.X. Xu, K.X. Sheng, C. Li, G.Q. Shi, Self-Assembled graphene hydrogel via a one-step hydrothermal process, ACS Nano 4 (7) (2010) 4324–4330.

[44] X. Xu, H. Li, Q.Q. Zhang, H. Hu, Z.B. Zhao, J.H. Li, J.Y. Li, Y. Qiao, Y. Gogotsi, Self-sensing, ultralight, and conductive 3D graphene/iron oxide aerogel elastomer deformable in a magnetic field, ACS Nano 9 (4) (2015) 3969–3977.

[45] Z.Y. Wang, X. Shen, M.A. Garakani, X.Y. Lin, Y. Wu, X. Liu, X.Y. Sun, J.K. Kim, Graphene aerogel/epoxy composites with exceptional anisotropic structure and properties, ACS Appl. Mater. Interfaces 7 (9) (2015) 5538–5549.

[46] P.F. Liu, F. An, X.Y. L, X.F. Li, P. Min, C. Shu, W. Li, Z.Z. Yu, Variable densification of reduced graphene oxide foam into multifunctional high-performance graphene paper, Compos. Sci. Technol. 201 (2021), 108492.

[47] C. Shu, H.Y. Zhao, S. Zhao, W.C. Deng, P. Min, X.H. Lu, X.F. Li, Z.Z. Yu, Highly thermally conductive phase change composites with anisotropic graphene/cellulose nanofiber hybrid aerogels for efficient temperature regulation and solar-thermal-electric energy conversion applications, Composites, Part B 248 (2023), 110367.

[48] F. An, X.F. Li, P. Min, H.F. Li, Z. Dai, Z.Z. Yu, Highly anisotropic graphene/boron nitride hybrid aerogels with long-range ordered architecture and moderate density for highly thermally conductive composites, Carbon 126 (2018) 19–127.

[49] F. Xu, R.F. Chen, Z.S. Lin, X.X. Sun, S.S. Wang, W.L. Yin, Q.Y. Peng, Y.B. Li, X. D. He, Variable densification of reduced graphene oxide foam into multifunctional high-performance graphene paper, J. Mater. Chem. C 6 (45) (2018) 12321–12328.

[50] S.S. Wang, X.X. Sun, F. Xu, M.L. Yang, W.L. Yin, J.J. Li, Y.B. Li, Strong yet tough graphene/graphene oxide hybrid films, Carbon 179 (2021) 469–476.

[51] P. Li, Y.J. Liu, S.Y. Shi, Z. Xu, W.G. Ma, Z.Q. Wang, S.P. Liu, C. Gao, Highly crystalline graphene fibers with superior strength and conductivities by plasticization spinning, Adv. Funct. Mater. 30 (2020), 2006584.
[52] X.D. Zhang, Z.T. Zhang, H.Z. Wang, B.Y. Cao, Thermal interface materials with high thermal conductivity and low Young's modulus using a solid–liquid metal codoping strategy, ACS Appl. Mater. Interfaces 15 (2) (2023) 3534–3542.
[53] D. Chung, Performance of thermal interface materials, Small 18 (16) (2022), 2200693.
[54] R.S. Prasher, J. Shipley, S. Prstic, P. Koning, J.L. Wang, Thermal resistance of particle laden polymeric thermal interface materials, J. Heat Tran. 125 (6) (2003) 1170–1177.
[55] X.D. Zhang, Z.T. Zhang, H.Z. Wang, B.Y. Cao, Thermal interface materials with high thermal conductivity and low Young's modulus using a Solid−Liquid metal codoping strategy, ACS Appl. Mater. Interfaces 15 (2) (2023) 3534–3542.
[56] Y.Q. Guo, H. Qiu, K.P. Ruan, Y.L. Zhang, J.W. Gu, Hierarchically multifunctional polyimide composite films with strongly enhanced thermal conductivity, Nano-Micro Lett. 14 (26) (2022), 00767-4.
[57] L. Wang, Z.L. Ma, H. Qiu, Y. Zhang, Z. Yu, J.W. Gu, Significantly enhanced electromagnetic interference shielding performances of epoxy nanocomposites with long-range aligned lamellar structures, Nano-Micro Lett. 14 (224) (2022), 00949-8.
[58] H. Zhang, Q.X. He, H.T. Yu, M.M. Qin, Y.Y. Feng, W. Feng, A bioinspired polymer-based composite displaying both strong adhesion and anisotropic thermal conductivity, Adv. Funct. Mater. 33 (2023), 2211985.
[59] H. Jung, S. Yu, N.S. Bae, S.M. Cho, R.H. Kim, S.H. Cho, I. Hwang, B. Jeong, J. S. Ryu, J. Hwang, S.M. Hong, C.M. Koo, C. Park, High through-plane thermal conduction of graphene nanoflake filled polymer composites melt-processed in an L-shape kinked tube, ACS Appl. Mater. Interfaces 7 (28) (2015) 15256–15262.
[60] K.M.F. Shahil, A.A. Balandin, Balandin, Graphene-multilayer graphene nanocomposites as highly efficient thermal interface materials, Nano Lett. 12 (2) (2012) 861–867.
[61] H. Shen, J. Guo, H. Wang, N. Zhao, J. Xu, Bioinspired modification of h-BN for high thermal conductive composite films with aligned structure, ACS Appl. Mater. Interfaces 7 (10) (2015) 5701–5708.
[62] J. Chen, X.Y. Huang, Y.K. Zhu, P.K. Jiang, Cellulose nanofiber supported 3D interconnected BN nanosheets for epoxy nanocomposites with ultrahigh thermal management capability, Adv. Funct. Mater. 27 (2017), 1604754.
[63] J.K. Han, G.L. Du, W.W. Gao, H. Bai, An anisotropically high thermal conductive boron nitride/epoxy composite based on nacre-mimetic 3D network, Adv. Funct. Mater. 29 (13) (2019), 1900412.
[64] Z.H. Wu, C. Xu, C.Q. Ma, Z.B. Liu, H.M. Cheng, W.C. Ren, Synergistic effect of aligned graphene nanosheets in graphene foam for high-performance thermally conductive composites, Adv. Mater. 31 (2019), 1900199.
[65] N. Song, D.L. Cao, X. Luo, Q. Wang, P. Ding, L.Y. Shi, Highly thermally conductive polypropylene/graphene composites for thermal management, Compos. Appl. Sci. Manuf. 135 (2020), 105912.
[66] J. Ma, T. Shang, L. Ren, Y. Yao, T. Zhang, J. Xie, B. Zhang, X. Zeng, R. Sun, J.B. Xu, C.P. Wong, Through-plane assembly of carbon fibers into 3D skeleton achieving enhanced thermal conductivity of a thermal interface material, Chem. Eng. J. 380 (2020), 122550.
[67] B. Ghosh, F. Xu, D.M. Grant, P. Giangrande, C. Gerada, M.W. George, X.H. Hou, Highly ordered BN⊥–BN⊥ stacking structure for improved thermally conductive polymer composites, Advanced Electronic Materials 6 (11) (2020), 2000627.
[68] L.C. Jia, Y.F. Jin, J.W. Ren, L.H. Zhao, D.X. Yan, Z.M. Li, Highly thermally conductive liquid metal-based composites with superior thermostability for thermal management, J. Mater. Chem. C 9 (8) (2021) 2904–2911.
[69] C.W. Nan, R. Birringer, D.R. Clarke, H. Gleiter, Effective thermal conductivity of particulate composites with interfacial thermal resistance, J. Appl. Phys. 81 (1997) 6692.
[70] Y. Cai, H.T. Yu, C. Chen, Y.Y. Feng, M.M. Qin, W. Feng, Improved thermal conductivities of vertically aligned carbon nanotube arrays using three-dimensional carbon nanotube networks, Carbon 196 (2022) 902–912.
[71] H.T. Yu, P.L. Guo, M.M. Qin, G.Y. Han, L. Chen, Y.Y. Feng, W. Feng, Highly thermally conductive polymer composite enhanced by two-level adjustable boron nitride network with leaf venation structure, Compos. Sci. Technol. 222 (2022), 109406.